ELECTRONIC BAND STRUCTURE AND P-DOS CALCULATION OF $CaReN_3$ SEMI-CONDUCTOR PEROVSKITE MATERIAL

Hardik Dave[1*] and Aditya Vora[2]

1. Abstract.

The total energy of $CaReN_3$ was calculated using the Quantum Espresso Simulation Package with the Perdew-Burke-Ernzerhof (PBE) wave function and 500 eV as a cut-off energy. The material posses a tetragonal shaped perovskite structure at 300K with the space group A2/n-15, consisting of Re-Ca bonds and a Ca-Re-N group. Optimization of cell characteristics along with atomic position is done. The band gap of $CaReN_3$, calculated using DFT-GGA-PBE, was found to be around 1.8 eV. The relativistic effects of the Re and Ca atoms significantly impact the band gap, which is typically underestimated by normal DFT calculations. In the range of UV, the $CaReN_3$ element used in optoelectronic devices due to its strong optical conductivity, low emissivity with high coefficient of absorption and raised refractive index. Less thean the band gap energy it exhibits transparent behaviour due to the incoming photon not having enough energy to move electrons between valence band and conduction band. The reflectivity spectra of $CaReN_3$ show that it has higher reflectivity than other semiconductors, with the highest peaks occurring in the energy gap of 2.5 eV to 21 eV.

[1*,2]Department of Physics, School of Science, Gujarat University, Navarangpura, Ahmedabad, Gujarat, India.

***Corresponding Author:** Hardik Dave
[*]Department of Physics, School of Science, Gujarat University, Navarangpura, Ahmedabad, Gujarat, India.
hardikdave3344@gmail.com

DOI: 10.48047/ecb/2023.12.si10.00284

2. Introduction.

Nitride materials are used in a variety of technological and industrial applications and are typically divided in-to following two categories. The main group metal nitride is included in the first group with crystal structures of wurtzite, such as (Ga, In, Al) N, they have strong carrier mobilities and straight bandgaps [3][4]. These materials have been seen very important in recent years due to their use in RF transistors, LED lighting and optical storage media with high density capabilities[5]. Transition Metal nitrides in the form of rock- salts like TiN [6], CrN [8] and VN [7] is the category two. They are used in Hard Coadt in Industries and barriers for the diffuction in active semiconductor devices [9]. They exhibit metallic behavior due to the transion possible in d-shell metal and some may even exhibit transitions seen in superconductors at 20 K. Some exceptions, such as semiconducting rocksalt nitrides like ScN [10] and metallic wurtzite nitrides like ZnMoN2, these are unusual compared to the more widely used and technologically significant materials

3. First Principle Calculation

3.1Computational details.

With the help of Perdew-Burke-Ernzerhof (PBE) wave function with the generalized gradient approximation (GGA) functional[13] and Quantum Espresso Simulation Package, Material's total energy was calculated [12]. A cut-off energy of 500 eV is used to achieve the necessary precision. geometric structure was optimized using a convergence threshold of 105 eV and a force per atom of 0.01 eV A1 accuracy. Calculations were performed using a reciprocal space sample and G-centers in a 10 by 10 by 10 of Monkhorst-Pack k-point mesh in the Brillouin zone[14].

4. Discussion and the results.

4.1Structural properties

$CaReN_3$ has a perovskite structure with the space group A2/n-15 at 300 K. The structure as well as optoelectronic properties of material $CaReN_3$ is influenced by its polarization. Other properties like Lattice structure, Phase transitions, Band gap and the Total energy are also affected. Calculation of Total energy based on first principle were performed on various arrangements of $CaReN_3$ to determine the preferred orientation of the cation. The $CaReN_3$ molecule has two Re-Ca bonds and the Ca-Re-N group forms a 128 degree angle. The molecule was placed in the unit cell by aligning the three nitrogen atoms in specific orientations. To reach to minimum energy the atom's shell made full to the ground level with exception of those forming the tetragonal cell shape. Three different local minima were obtained by orienting the $CaReN_3$ molecule along different single crystal orientations. This is in contrast to $CaReN_3$, which has a single Re-Ca bond with a unique polarization orientation.

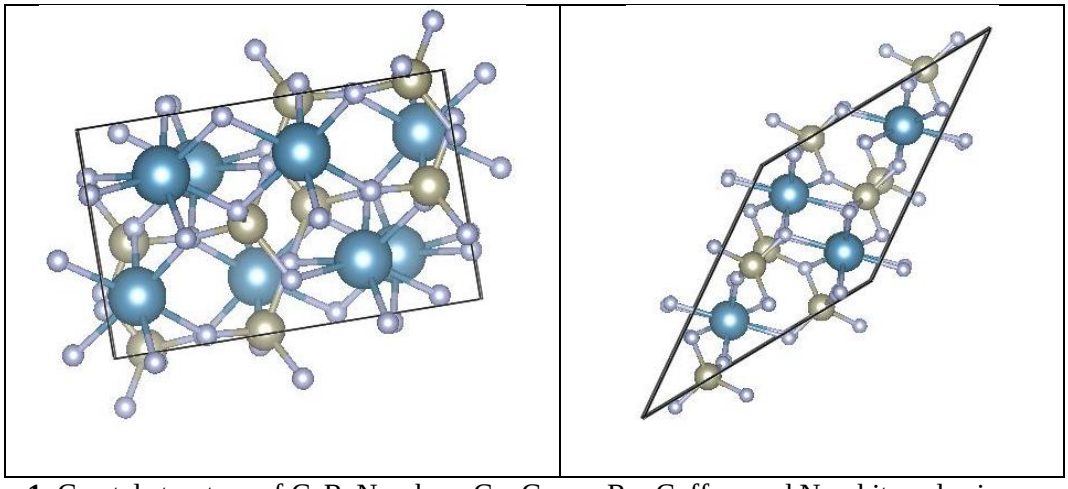

Figure 1. Crystal structure of $CaReN_3$ where Ca: Green, Re: Coffee, and N: white color in represents.

4.2 Electronic properties

Atomic position along with characteristics of cell optimised geometrically using: GGA-PBE-DFT methods. When the results of these calculations were compared, Bandgap accuracy of 1.8 eV is obtained through DFT-PBE method. This high level of precision was largely due to Re atom's relativistic behaviour, which compensated standard DFT methods offer under estinmated band gap. The GGA-PBE method was used to obtain a precise band gap measurements. However, spin-orbit coupling (SOC) was not included in these GW calculations due to the demanding computational requirements of the technique for $CaReN_3$ tetragonal type perovskitesemiconductor material.

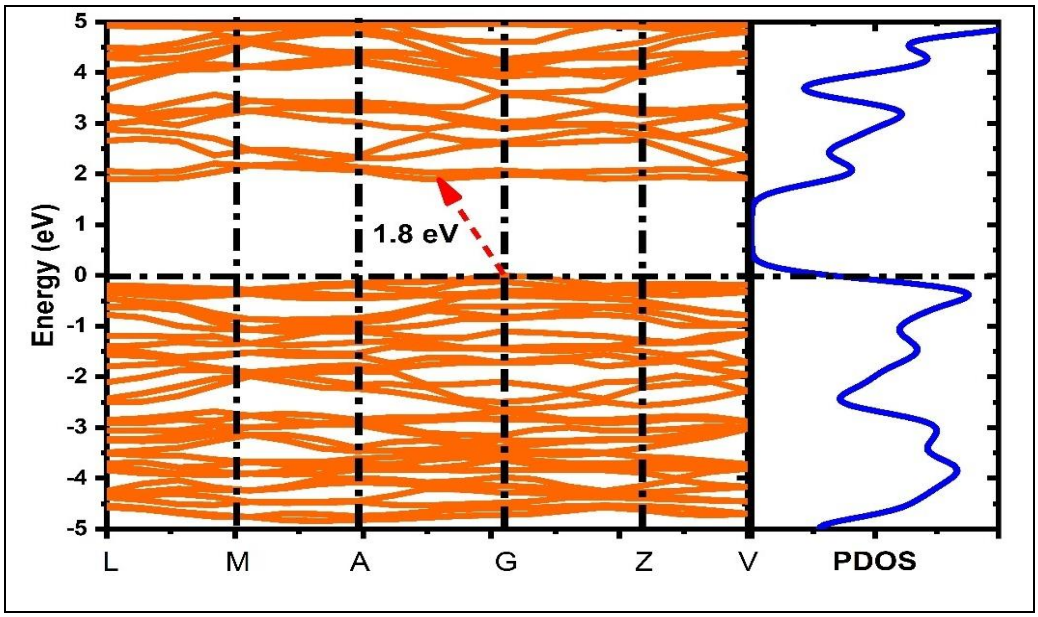

Figure 2. Electronic band structure calculation of High symmetric Point L to V of

The VBM (valence band maximum) and CBM (conduction band minimum) are both located at the G point (0.5 0.5 0.5). As shown in Figure 2, the introduction of the Re atom significantly reduces the forbidden gap of $CaReN_3$. The value of separation of bansd is around 1.8 eVwhen calculated using above methods. Re and Ca atom's relativistic behaviour, which compensated standard DFT methods offer under estinmated band gap [15], resulting into perfect match with observed values in DFT analysis. This perfect calculation of the band-gap energy are even observed in $CaReN_3$, a standard Ca-included tetragonal perovskite structure. It suggests that GGA-PBE can provide a reliable approximation method of the band gap and electronic configuration in $CaReN_3$ generally[16].

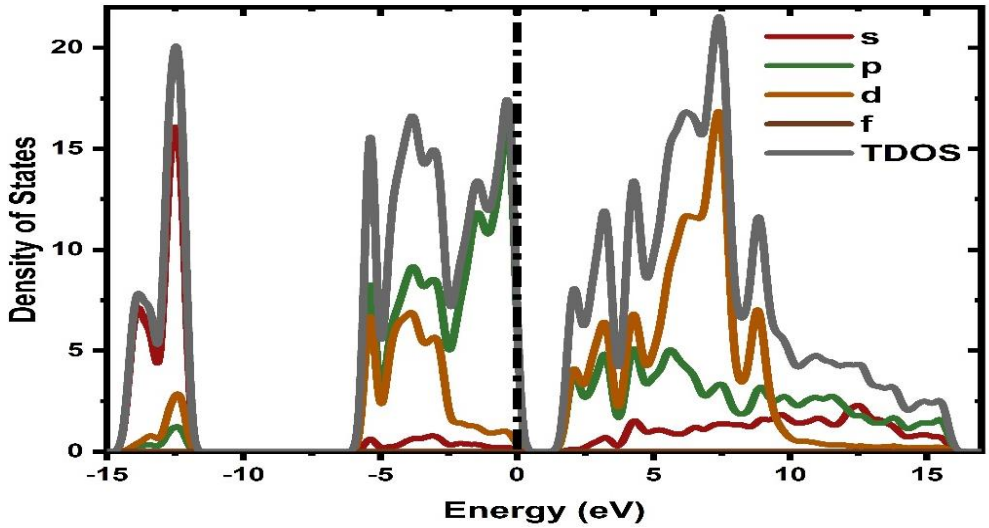

Figure 3. P—DOS calculation of $CaReN_3$ tetragonal type perovskite semiconductor.

The Net projected DOS (Density of State) of $CaReN_3$ in cubical shape, was estimated by the DFT-PBE Method, are shown in Fig. 3. These calculations indicate that in $CaReN_3$, Re donates one electron and the two Ca ions donate one electron each, by creating an energy gap between vacant 6p orbital of Re atom in CB and filled 6p of Ca and 3p of N of valance band., which agrees the experimental conclusions for $CaReN_3$[17]. However, the changes in orbital character are due to the variations between the $CaReN_3$ molecules. The $CaReN_3$ exhibits DOS peaks between 2.5 and 10 eV due to the 2p and 3d of Ca, Re, and Nitrogen, while exhibiting orbitals around energy level of 5 eV. Net projected DOS (Density of State) of $CaReN_3$ of tetragonal $CaReN_3$, estimated by GGA-PBE approach, are shown in Fig. 3. These calculations show that in $CaReN_3$, Ca and Re

donate one-two electrons each, to 3- Nitrogen ions, that creats energy gap in empty 5d of Re orbitals of CB and filled 6p of Ca and 2p of N orbitals in the VB.

5. Optical Properties:

The frequency response of a material's optical properties to the energy of the incident photon (E=hv) is described using the material's optical properties. The frequency-dependent complex dielectric function can be used to determine the different optical parameters of any material. The complex dielectric function can be expressed using the following equation:

$$\varepsilon(\omega)+\varepsilon_1(\omega)+i\varepsilon_2(\omega) \text{ ……..(1)}$$

The electronic band structure and dielectric function of a material are closely related. The imaginary component $(\varepsilon_2(\omega))$ of the dielectric function [19] can be calculated using the following equation:

$$\varepsilon_2(\omega)=\frac{8\pi^2e^2}{\omega^2m^2}\sum_n\sum_{n'}\int|P^v_{nn'}(k)|^2\ f_{kn}(1-f_{nn'})\delta(E^k_n-E^k_{n'}-\hbar\omega)\frac{d^3k}{(2\pi)^3} \text{ ……(2)}$$

Where;

$P^v_{nn'}$ k – component of P dipole matrix on direction of E filed v between the final and initial states,

f_{kn} - Fermi and Dirac distribution,

$E^k_{n'}$ (k) – electron's energy

M -mass of electron

e- charge of an electron

$\varepsilon_2(\omega)$ depends on angular frequency and is imaginary part of of the dielectric constant $\varepsilon(\omega)$. Real part $\varepsilon_1(\omega)$ can be deduced through it via the Kramers-Kronig transformation[20].

$$\varepsilon_1(\omega)=1+\frac{2}{\pi}P\int_0^\infty\frac{\omega'\varepsilon_2(\omega')}{\omega'^2-\omega^2}d\omega' \text{ ……..(3)}$$

Finally, Values of the dielectric function's real part $\varepsilon_1(\omega)$ on the y-axis of the chart depicted in fig 4. $\varepsilon=0$ are known as constant of real part $\varepsilon_1(\omega)$. Figure 4.shows that the static values of real component $\varepsilon_1(\omega)$ for $CaReN_3$ are around 4 eV & 7 eV each. The spectra of $CaReN_3$ is virtually identical in pattern, with minor anisotropy evidenced by shifting peak height and location. $CaReN_3$ exhibit reflection of light particle at high intensity because the $\varepsilon_1=0$ of the $\varepsilon(\omega)$ becomes -ve around 10 eV.

Electronic characteristics of crystalline materials are primarily defined using the imaginary component $\varepsilon_2(\omega)$ of $\varepsilon(\omega)$, it is responsible for absorption of photon. Figure 4 shows estimated $(\varepsilon_2(\omega))$ spectrum for $CaReN_3$[21]. The cut off value of $(\varepsilon_2(\omega))$ is obtained using GGA-PBE method where the heighted first value is at 5 eV and 7.7EV for $CaReN_3$. This peak values arised due to imaginaray component as a result of electron transitions from the VB to CB. For both substances, the maximum value of $(\varepsilon_2(\omega))$ is about 5 eV. Following that, as energy increases, the spectra of both substances diminish. Elecronic enery bands can exhibits transition between valence to conduction band in the form of optical transistion. Such type of the first one occurs in between universal VBM and CBM in theΓ- Γdirection.

Coefficient of absorption, refractive index, coefficient of reflection and energy loss fuction etc characteristics can be deduced with the help of dielectric constant. [22]. Using the estimated values of $\varepsilon_1(\omega)$ and $(\varepsilon_2(\omega))$, the following relationship is used to derive the refractive index of the mensioned materials (w)

$$n(\omega)=\left[\frac{\sqrt{\varepsilon_1^2(\omega)+\varepsilon_1^2(\omega)}}{2}+\frac{\varepsilon_1(\omega)}{2}\right]^{1/2}$$

……(4).

With the help of dielectric function, refractive index n(0) can be obtained. [23].

$$n(0)=\sqrt{\varepsilon_1(0)} \text{ ……..(5).}$$

To obtain frequency-dependent extinction coefficient $(k=\omega)$ help of The Kramers Kronig transformation is taken, which can be related to the refractive index $n=\omega$.

$$k(\omega) = -\frac{2p}{\pi}\int_{\infty}^{0}\frac{n(\omega')-1}{\omega'-\omega}d\omega' \text{ .....(6).}$$

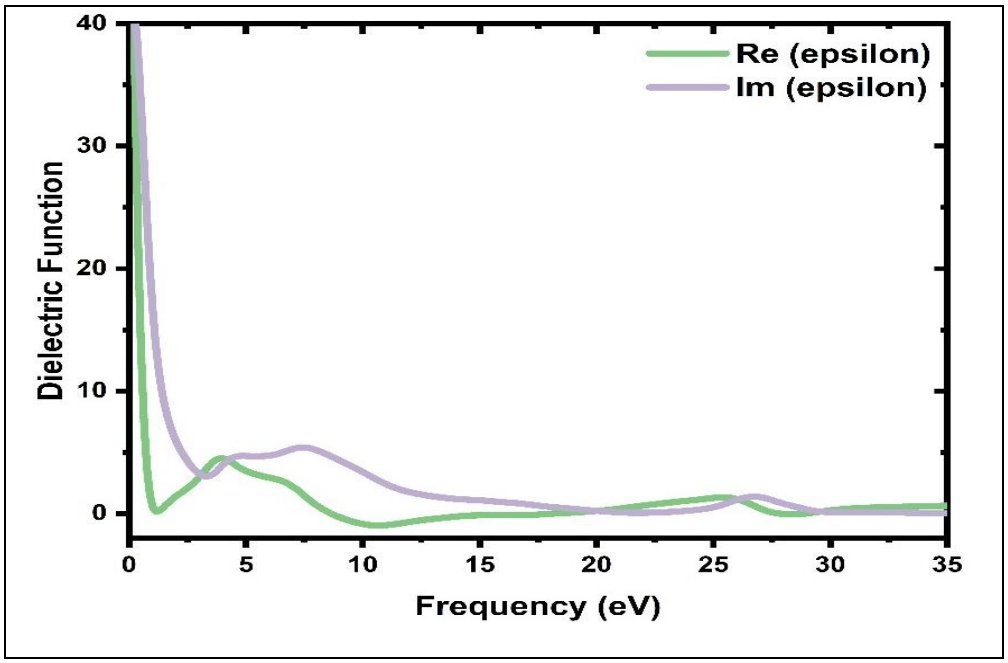

Figure 4. Real (Re) and Imaginary (Im) of part of dielectric function for

Behaviour of $(k(\omega))$ is analysed with the help of $(k(\omega))$ (Calculated extinction coefficient) and $k_{\max}(\omega)$. Complex form of RI (Refractive Index) $N(\omega) = n(\omega) + ik(\omega)$ if helpful to expain the motion of EM radiation in different material. [24].

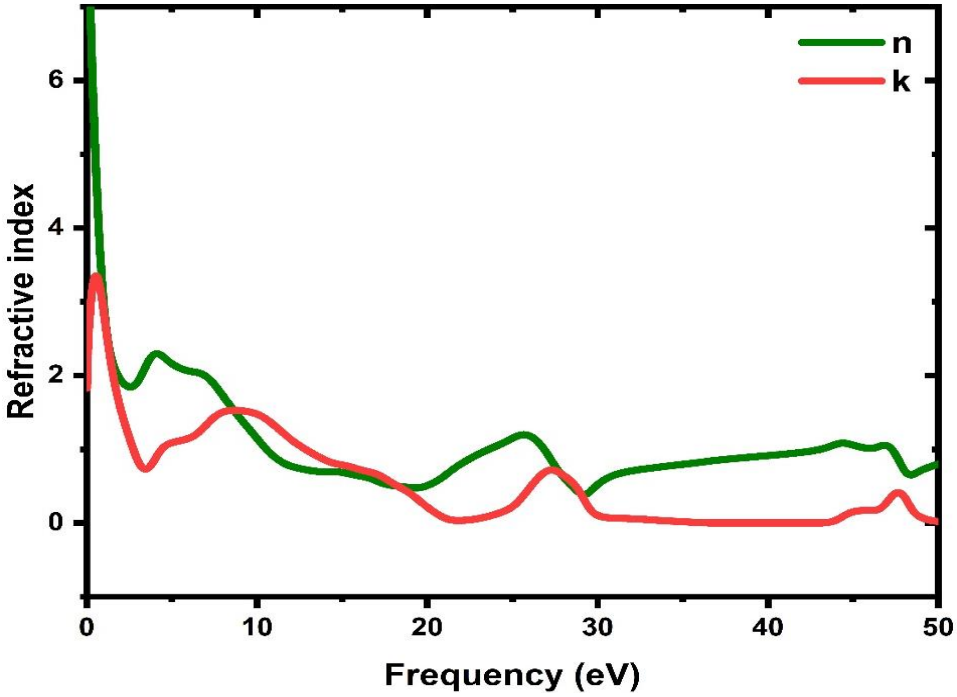

Figure 5. Reflactive Index of $CaReN_3$ seiconductor material

For evaluation of devices such rexfractive indices are used. The materials used in photo cell or such systems should be having higher optical conduction, refractive index & absorption constant with less emissivity. Figure 5(a) and (b) exhibit spectrum $n(\omega)$ and $k(\omega)$ computed by the GGA-PBE method for $CaReN_3$. $n(0)$ static refractive index values of $CaReN_3$ are roughly 2.1 and 3.5, respectively. The maximum refractive index

$(n(\omega))$ values for $CaReN_3$ are 15 eV and 17 eV, respectively.

Figures 5 (a) and 5(b) show a comparable profile of the real component $\varepsilon_1(\omega)$ and the $n(\omega)$ (refractive index). Photons of less low energy have the first peak in both spectrums. After the initial peak caused by fluctuations, the spectra of both coefficients show a gradual decrease.

Imaginary component $\varepsilon_2(\omega)$ of dielectric constant and Extinction coefficient $(k(\omega))$ have comparable profiles, as seen in Fig 5(a) and Fig 4(a). $k(\omega)$ also begins at some threshold energy, comparable to the imaginary component $\varepsilon_2(\omega)$ of $\varepsilon(\omega)$. The threshold values of energy for extinction coefficient $(k(\omega))$ for $CaReN_3$ are around 10 eV and 26.5 eV, respectively.

The maximum extinction coefficients $k_{max}(\omega)$ for $CaReN_3$ are 2.5eV and 3.5 eV, respectively. Reaching to maximum values, $k(\omega)$ spectrum declines towards unity.

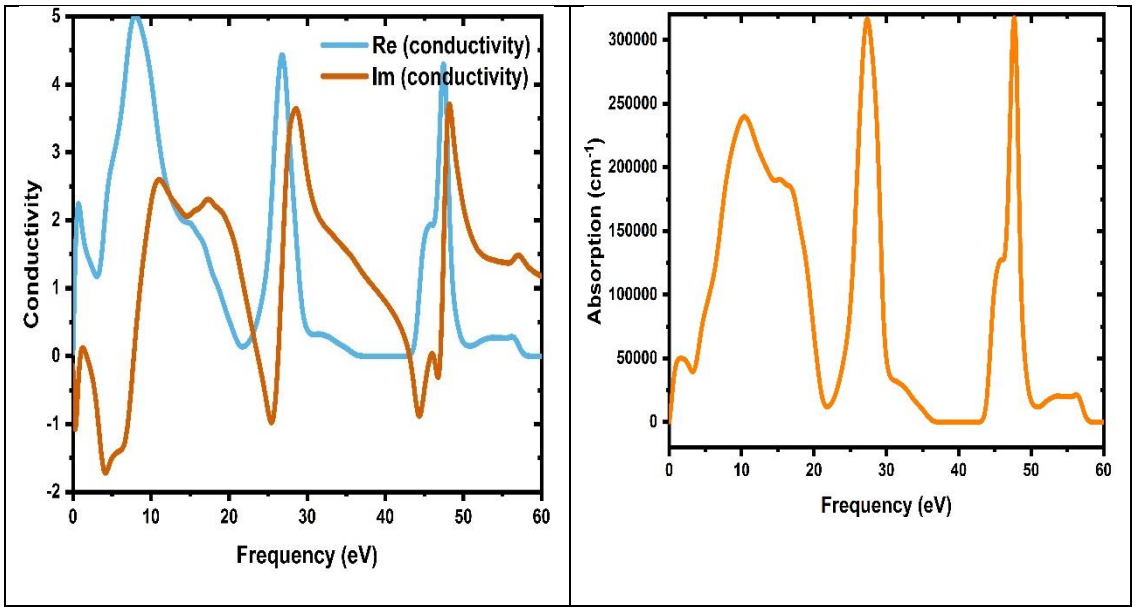

Figure 6. Conductivity(a) and Absorption (b) of $CaReN_3$

Figure 6 shows the spectrum of the $I(\omega)$ (absorption coefficient) computed by the GGA-PBE approximation. Calculations demonstrate they exhibit transparent behaviour lower the energy gap (VB- Valence Band), as illustrated in Fig. 6(a), because bombarded photon's energy is insufficient to move electron Conduction band from valence band. Fig. 6 depicts presence of anisotropy in absorption coefficients of $CaReN_3$. Absorption coefficient is greatly affected by frequency, indicating that interaction of photon with electrons make them to move to conduction band from valance band.

Range from 0 to 60 eV, Absorption coefficient of $CaReN_3$ as a whole is larger than the absorption coefficient. These findings indicate that $CaReN_3$ are viable options in UV range to the optoelectronic devices. Fig 6(a) shows that the greatest values of $I(\omega)$ for $CaReN_3$ is about 3.5 to 10 eV. Absorption co-eff. is found greatest to 27 eV and 46 eV for $CaReN_3$.

Reflectivity $R(\omega)$ is calculated using refractive index $(n(\omega))$ and extinction coefficient $(k(\omega))$ of above mensioned compounds by following equation;[25].

$$R(\omega) = \frac{(1-n)^2 + k^2}{(1+n)^2 + k^2} \quad \text{.....(7)}$$

Using the following relationship, Reflectivity as a function of frequency can be obtained using dielectric function as follows[26]

$$R(\omega) = \left| \frac{1-\sqrt{\varepsilon(\omega)}}{1+\sqrt{\varepsilon(\omega)}} \right| \quad \text{.....(8)}$$

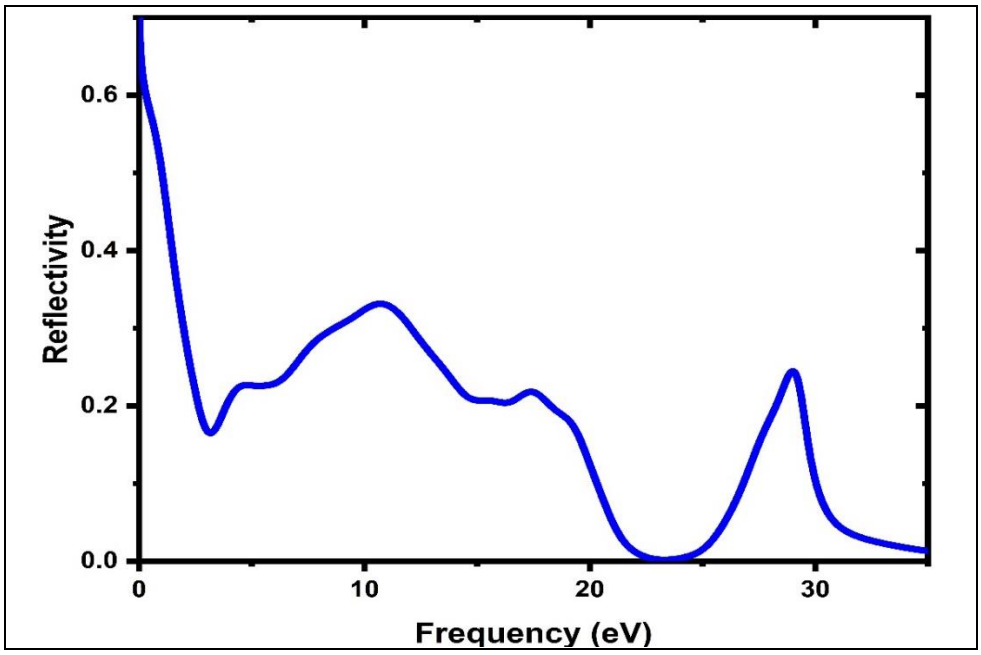

Figure 7. Reflectivity of $CaReN_3$ semiconductor material

Figure 7. shows the chart of reflectivity as a function of frequency $R(\omega)$ w for $CaReN_3$. Figure 7 shows that the static reflectivity n(0) values for $CaReN_3$ is 0.31. The spectra demonstrate that $CaReN_3$ has a greater reflectivity. The highest peaks of reflectivity as a function of frequency $R(\omega)$ spectrum of $CaReN_3$ may be found in the energy range of 2.5 eV through 21 eV. Greatest value of reflectance $R(\omega)$ values for $CaReN_3$ are 0.35 and 0.27, respectively.

The energy loss function $L(\omega)$ describes the energy dissipation is caused by electrons across the matter. Using the following relationship, Dissipation of energy can be calculated using given formula consisting complex refractive index[27].

$$L(\omega) = In\left(-\frac{1}{\varepsilon(\omega)}\right) \ldots\ldots\ldots\ldots (9)$$

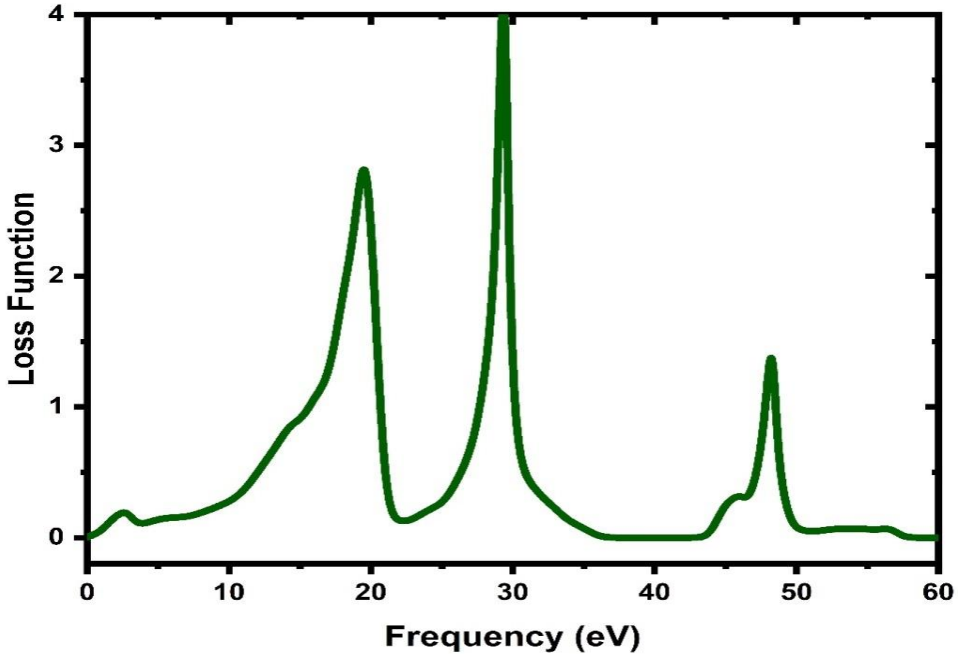

Figure 8 Energy loss function for $CaReN_3$

Figure 8 depicts calculated spectrum of dissipated energy through the range of 0 eV to 60 eV. It intrepretes the interaction of photon with electrons very well. It provides $L(\omega)$ provides useful information on the interaction of incoming photons with electronic devices. There is depression seen in

reflectivity spectrum at the same time. Existence of strong rise at 19 and 29.1 eV for the energy loss function $L(\omega)$ is an important feature. Resonance of Plasma occurs at plasma frequency in $CaReN_3$.

Conclusion.

Both, Electronic as well as optic based properties of $CaReN_3$ has been studied by a DFT-based generalized gradient schemes GGA-PBE methods . Direct energy gap (Γ-Γ)has been revealed for mensioned compound. Precised estimation of electronic configuration along with structures of band and total and partial DOS, were analysed by the GGA approaximation. Dielectric function revealed compountd's optical characteristic and behaviour. The important peaks in the dielectric functions are due to transition of electrons from the Ca-Re-N and Re-N orbitals. The variations of the dielectric functions and other optical properties depend on materials energy level diffrences, with an contarary behaviour for band gap and a similar nature for the threshold frequency or critical point in the spectra. Tuning the band gap of optica properties of materials depends on their types and nature and can guide towards to the development ofmore reliable and efficient opto/lumino based devices operating in the various region of radiation spectrum. They have also responded strongly for the absorption to UV and visible region of radiation, making them preferable for solar power generation related devices. In addition, Diffrence in absorption in these materials may have potential uses the field of polarisation and filteration. The materialshave shown great reflectance to ultraviolet, indicating their potential use for ultraviolet shielding. This research searves as new material and its manufacturing in many appications. Use of Nitrogen for improving their optoelectric capabilities is inevitable.

6. References.

1. J. A. Garrido, E. Mun, and J. L. Sa, "Tailoring of internal fields in AlGaN/GaN and InGaN/GaN heterostructure devices ˜," vol. 61, no. 4, pp. 2773–2778, 2000.
2. X. Wang, W. Liu, C. Zhai, J. Yun, and Z. Zhang, "DFT calculation on the electronic structure and optical properties of InxGa1-xN alloy semiconductors," *Medziagotyra*, vol. 26, no. 2, pp. 127–132, 2020, doi: 10.5755/ j01.ms.26.2.21569.
3. A. Belabbes, J. Furthmüller, and F. Bechstedt, "Relation between spontaneous polarization and crystal field from first principles," *Phys. Rev. B - Condens. Matter Mater. Phys.*, vol. 87, no. 3, pp. 1–6, 2013, doi: 10.1103/ PhysRevB.87.035305.
4. A. Chaiken *et al.*, "Structural and Electronic Properties of Amorphous and Polycrystalline In2Se3 Films," vol. 2390, no. 2003, 2003, doi: 10.1063/1.1592631.
5. H. H. Amer, M. Elkordy, M. Zien, A. Dahshan, and R. A. Elshamy, "Characterization of quaternary chalcogenide As-Ge-Te-Si thin films," *Optoelectron. Adv. Mater. Rapid Commun.*, vol. 5, no. 4, pp. 381–386, 2011.
6. V. Rawat, D. N. Zakharov, E. A. Stach, T. D. Sands, and W. Lafayette, "Pseudomorphic stabilization of rocksalt GaN in TiN / GaN multilayers and superlattices," pp. 1–5, 2009, doi: 10.1103/PhysRevB.80.024114.
7. F. Padera, "Measuring Absorptance and Refractive Index of Thin Films with the PerkinElmer Lambda 950/1050 High Performance UV-Vis/NIR Spectrometers," pp. 1–9, 2013, [Online]. Available: http:// www.perkinelmer.com/CMSResources/Images/44-153901APP_Thin-films.pdf.
8. S. K. Gupta, S. D. Gupta, H. R. Soni, V. Mankad, and P. K. Jha, "First-principles studies of the superconductivity and vibrational properties of transition-metal nitrides TMN (TM ¼ Ti , V , and Cr)," *Mater. Chem. Phys.*, vol. 143, no. 2, pp. 503–513, 2014, doi: 10.1016/j.matchemphys. 2013. 08.046.
9. A.P.Kochuparampil,J.H.JoshiandM.J.Joshi," Growth,structural,spectroscopic,thermal,dielectric and optical studyof cobalt sulphide - doped ADP crystals",modern physics letters B,vol.31,no.27,2017,doi:10.1142/S0217984917502463.
10. M. El-Hagary, M. Emam-Ismail, E. R. Shaaban, A. Al-Rashidi, and S. Althoyaib, "Composition, annealing and thickness dependence of structural and optical studies on Zn1-xMnxS nanocrystalline semiconductor thin films," *Mater. Chem. Phys.*, vol. 132, no. 2–3, pp. 581–590, 2012, doi: 10.1016/ j. matchemphys.2011.11.072.
11. K. Hasanirokh, A. Asgari, and M. Mahdizadeh Rokhi, "Theoretical study on nonlinear optical properties of CdS/ZnS spherical quantum dots," *Optik (Stuttg).*, 2019, doi: 10.1016/ j. ijleo.2019.03.053.
12. P. Giannozzi, "Quantum simulations of materials using quantum ESPRESSO," p. 40, 2012.
13. J. P. Perdew *et al.*, "Erratum: Atoms, molecules, solids, and surfaces: Applications of the generalized gradient approximation for exchange and correlation (Physical Review B (1993) 48, 7, (4978))," *Phys. Rev. B*, vol. 48,

no. 7, p. 4978, 1993, doi: 10.1103/ PhysRevB. 48.4978.2.

14. H. J. Monkhorst and J. D. Pack, "Special points for {B}rillouin-zone integrations," *Phys. Rev. B*, vol. 13, pp. 5188–5192, 1976.
15. S. Zhang, N. S. A. Alt, E. Schlücker, and R. Niewa, "Novel alkali metal amidogallates as intermediates in ammonothermal GaN crystal growth," *J. Cryst. Growth*, vol. 403, pp. 22–28, 2014, doi: 10.1016/ j.jcrysgro. 2014. 06. 015.
16. D. Zhou, L. Zhao, and B. Li, "Recent progress in solution assembly of 2D materials for wearable energy storage applications," vol. 62, pp. 27–42, 2021, doi: 10.1016/ j.jechem. 2021.03.002.
17. D. J. Kubicki, D. Prochowicz, A. Hofstetter, S. M. Zakeeruddin, M. Grätzel, and L. Emsley, "Phase Segregation in Cs-, Rb- and K-Doped Mixed-Cation (MA)x(FA)1-xPbI3 Hybrid Perovskites from Solid-State NMR," *J. Am. Chem. Soc.*, vol. 139, no. 40, pp. 14173–14180, 2017, doi: 10.1021/jacs.7b07223.
18. M. Souleiman *et al.*, "Hydrothermal growth of large piezoelectric single crystals of GaAsO 4," *J. Cryst. Growth*, vol. 397, pp. 29–38, 2014, doi: 10.1016/j.jcrysgro.2014.03.046.
19. J. A. Phys, "Structural , optical , transport , and solar cell properties of 2D halide perovskite MAZX 3 (Z = Pb , Sn , and X = Cl , Br , I) Structural , optical , transport , and solar cell properties of 2D halide perovskite MAZX 3 (Z = Pb , Sn , and X = Cl , Br ," vol. 3, no. June, 2020, doi: 10.1063/5.0016331.
20. S. Berri, "First-principles calculations to investigate structural, electronic, half-metallic and thermodynamic properties of hexagonal UX2O6 (X=Cr,V) compounds," *J. Sci. Adv. Mater. Devices*, vol. 4, no. 2, pp. 319–326, 2019, doi: 10.1016/j.jsamd.2019.05.002.
21. M. Safaei, H. A. Sodano, and S. R. Anton, "A review of energy harvesting using piezoelectric materials: State-of-the-art a decade later (2008-2018)," *Smart Mater. Struct.*, vol. 28, no. 11, 2019, doi: 10.1088/ 1361-665X/ab36e4.
22. M. L. Liang, C. L. Hu, F. Kong, and J. G. Mao, "BiFSeO3: An Excellent SHG Material Designed by Aliovalent Substitution," *J. Am. Chem. Soc.*, vol. 138, no. 30, pp. 9433–9436, 2016, doi: 10.1021/jacs.6b06680.
23. D. Singh, S. K. Gupta, H. He, and Y. Sonvane, "First-principles Study of the Electronic , Magnetic and Optical Properties of Fe 3 Se 4 in its Monoclinic Phase," *J. Magn. Magn. Mater.*, p. 166157, 2019, doi: 10.1016/j. jmmm.2019.166157.
24. S. Sahu and M. Zwolak, "Colloquium: Ionic phenomena in nanoscale pores through 2D materials," *Rev. Mod. Phys.*, vol. 91, no. 2, p. 21004, 2019, doi: 10.1103/RevModPhys. 91.021004.
25. R. Ahmed *et al.*, "Investigations of electronic and thermoelectric properties of half-Heusler alloys XMgN (X = Li, Na, K) by first-principles calculations," *Mater. Des.*, vol. 136, pp. 196–203, 2017, doi: 10.1016/j.matdes 2017.09.038.
26. M. Gao, Q. Li, X. Yan, and J. Wang, "Prediction of phonon-mediated supercon ductivity in borophene," vol. 024505, pp. 1–9, 2017, doi: 10.1103/PhysRev B.95. 024505.
27. K. Hayat, M. A. Rafiq, S. K. Durrani, and M. M. Hasan, "Impedance spectroscopy and investigation of conduction mechanism in BaMnO3 nanorods," *Phys. B Condens. Matter*, vol. 406, no. 3, pp. 309–314, 2011, doi: 10.1016/j.physb.2010.09.026.